Applied Physics B (2022) 128:202
https://doi.org/10.1007/s00340-022-07923-7

Applied Physics B
Lasers and Optics

RESEARCH

Third harmonic generation in the thin films containing quantum dots and exfoliated nanoparticles

R. A. Ganeev[1,2,3] · V. V. Kim[1] · I. A. Shuklov[4] · V. S. Popov[4] · N. A. Lavrentyev[4] · V. P. Ponomarenko[4] · A. A. Mardini[4] · D. V. Dyomkin[4] · T. Milenkovič[4] · A. Bundulis[5] · J. Grube[5] · A. Sarakovskis[5]

Received: 20 July 2022 / Accepted: 10 October 2022 / Published online: 15 October 2022

Abstract
We demonstrate high conversion efficiency towards the third harmonic (TH) of the 900–1700 nm, 150 fs laser in the thin (40–120 nm) films containing quantum dots (HgTe, HgSe, and PbS) and exfoliated nanoparticles (Bi_2Te_3) deposited on the glass substrates. The ratio of TH conversion efficiencies in the films and glasses of the same thickness was estimated to be $> 10^4$. The intensity, polarization, and spectral dependencies of this process in thin films are reported. We discuss the relation between the TH process and the low-order nonlinear optical properties of these quantum dots and nanoparticles.

1 Introduction

The growing interest in quantum dots (QDs) and exfoliated topological insulator nanoparticles (NPs) is attributed, particularly, due to their large low-order optical nonlinearities, which can be useful in photonics and optoelectronic devices in different time scales. QDs and NPs have properties intermediate between bulk semiconductors and discrete atoms or molecules. Their characteristics change as a function of both size and shape [1].

The detailed theoretical studies of the electronic structure of (InGa)(AsSb)/GaAs/GaP and other QDs are presented in [2]. These systems are unique since they exhibit concurrently direct and indirect transitions both in real and momentum space and are attractive for applications in quantum information technology. The effect of Coulomb correlation on the emission properties of the ground state exciton in zincblende CdSe/ZnS core–shell and in wurtzite ZnO QDs is analyzed in [3]. Other theoretical studies of QDs include those considering the exciton and biexciton energies calculated using the envelope function approximation and the configuration interaction method [4], the polarization response of the emission from type-II GaAsSb capped InAs QDs [5], calculations based on the interaction method showing excellent quantitative agreement with the experiment and allowing to elucidate the role of Coulomb interactions among the confined particles and of electronic correlation effects on the Stark shifts [6], detailed theoretical studies of the magneto-optical properties of weakly confining GaAs/AlGaAs QDs [7], and the structural analysis of the ground-state exciton of Cd(Se,Te)QDs embedded in ZnTe matrix using configuration interaction method [8].

Semiconductor QDs can find their use in nonlinear optical applications due to the spike-like density of their electronic states. The concentration of optical transitions in very narrow energy intervals in QDs causes a strong enhancement of the nonlinear optical response [9, 10]. Weakly confined QDs have been studied in more detail for a variety of materials (such as CdS, CdSe, Ag_2S or $CsPbBr_3$) [11, 12]. The available studies of strongly confined QDs are mostly limited to PbSe and PbS [13, 14]. Core–shell materials have also been investigated for nonlinearities [14, 15]. Nonlinear optical effects should be more pronounced in the QDs, which demonstrate stronger confinement properties compared with the

✉ R. A. Ganeev
rashid.ganeev@lu.lv

✉ I. A. Shuklov
shuklov.ia@mipt.ru

1 Laboratory of Nonlinear Optics, University of Latvia, Jelgavas 3, Riga 1004, LV, Latvia

2 Tashkent Institute of Irrigation and Agricultural Mechanization Engineers, National Research University, Kori Niyozov Street 39, Tashkent, Uzbekistan 100000

3 Department of Physics, Voronezh State University, Voronezh 394006, Russia

4 Moscow Institute of Physics and Technology (National Research University), Dolgoprudny 141701, Russia

5 Institute of Solid State Physics, University of Latvia, Kengaraga 8, Riga 1063, LV, Latvia

NPs. Particularly, lead sulfide (PbS) QDs are an excellent model object for studying physical processes in a strong confinement regime [16]. The large exciton Bohr radius (18 nm) of PbS allows to investigate the size dependencies of linear and nonlinear optical properties under the strong confinement for a variety of QD sizes, minimizing the contribution from surface-related effects.

The importance of the development of low-dimensional semiconductor structures in second-generation semiconductor materials for enriching nonlinear optical properties was also demonstrated in a few recent studies [17–19]. Novel synthesized semiconductor QDs and NPs require to be examined under different conditions using laser pulses of variable energies, wavelengths, and durations to understand the nonlinear optical mechanisms and distinguish the attractive properties of those processes for different practical applications [20–25]. The impressive third-order nonlinear optical properties make nanoscale species potentially useful in electroluminescent devices like light-emitting diodes and optical devices such as optical switchers.

In the present paper, we address another potential application of these small-sized nanocrystals. The goal of the present study is a demonstration of the efficient third-harmonic generation (THG) of the laser radiation propagating through these media formed in the shape of thin films. Special attention to the thin films containing these QDs is also related to the growth of the nonlinear refractive indices, nonlinear absorption coefficients, and saturation intensities. Quantum confinement is found to enhance the nonlinear optical response, and a number of reports have discussed the physical processes underlying the mechanism of optical nonlinearities in QDs. In these circumstances, one can expect that other components of third-order susceptibilities, particularly those responsible for the frequency conversion of fundamental radiation, can be also enhanced thus providing the opportunity for efficient generation of the lowest (third) harmonic.

THG in air and laser-induced plasmas using femtosecond pulses from Ti:sapphire lasers is a well-studied process that allows determining the maximally available conversion efficiency of this nonlinear optical effect and diminishing the impeding mechanisms restricting this process [26–30]. THG allows the formation of the coherent UV sources of femtosecond pulses at the conversion efficiency from 800-nm-class lasers of up to 10^{-3} [31–33] or even higher [34–36].

Below we analyze the films containing QDs (PbS, HgTe, HgSe) and exfoliated NPs (Be_2Te_3). We demonstrate high conversion efficiency towards the third harmonic (TH) of the tunable (900–1700 nm), 150 fs laser in the thin (40–120 nm) films containing these QDs and NPs deposited on the glass substrates. We show the high ratio of TH conversion efficiencies in films and glasses of the same thickness. The motivation of the present study is, particularly, related to the potential application of thin films containing QDs for high-order harmonics generation of ultrashort laser pulses. There are some assumptions about the correlation between the large yield of low-order harmonics and the high efficiency of higher-order harmonics in such structures. Thus one has to analyze the ability of the studied small-sized species to convert the wavelength of the interaction laser field using the lowest-order nonlinear optical process (THG).

2 Experimental

2.1 Preparation of films on the 0.15 mm thick silica glass plates

2.1.1 Bi_2Te_3 NPs

The details of Bi_2Te_3 NPs synthesis and characterization are presented elsewhere [37]. Since the quintuple layers (Te(1)–Bi–Te(2)–Bi–Te(1)) in a bismuth telluride crystal are connected by van der Waals forces, it becomes possible to obtain the suspensions of thin sheets of Bi_2Te_3 using simple exfoliation methods, as it was shown in [37].

Liquid-phase exfoliation (LPE) with a simple sonication bath (8 h, 30–45 °C) was used to obtain Bi_2Te_3 NPs suspension in butanol-2 (0.01 M) using Bi_2Te_3 powder as a source. 2D Bi_2Te_3 NPs were dip-coated on the 0.15 mm thin silica glass substrate with a withdrawal speed of 1.3 mm/h using suspension immediately after LPE.

In accordance with transmission electron microscopy (TEM) measurements, the thin two-dimensional sheets Bi_2Te_3 were obtained by LPE. Several 10–20 nm 2D-crystallites were aggregated in the larger-sized particles. The average thickness of obtained films was 40–50 nm.

2.1.2 HgTe QDs

The synthesis of mercury telluride QDs with narrow size distribution was performed by the hot-injection organometallic route. The tellurium precursor reacted with mercury halides at lower temperatures (60–80 °C) in comparison with cadmium (250 °C) or lead (180 °C) during the preparation of the tellurides. Short reaction times and temperatures as low as 60 °C allowed us to obtain the small-sizes HgTe QDs capped with 1-dodecanethiol. We obtained good stability of the colloidal solutions [38].

TEM measurements of these QDs allowed for determining their mean diameter (4 nm). The optical absorption of prepared QD suspension showed stronger absorbance at 500 nm compared with the 1000 nm spectral region. The preparation of thin films was carried out layer-by-layer using dip-coating with a withdrawal speed of 30 mm/min from tetrachloroethylene colloidal solution on the glass substrate. The original ligand shell was exchanged for

1,2-ethanedithiol. The thickness of the HgTe QD films deposited on the 0.15 mm plates was ~ 70 nm.

2.1.3 PbS QDs

The long-term stable colloidal solutions were obtained by replacement of the original ligand shell by the oleate using the oleic acid. The PbS colloidal QDs synthesized by this method were stable for a few weeks. The preparation of small-sized PbS QDs was performed in an argon atmosphere to avoid oxidation. Firstly, the sulfur precursor was prepared by dissolving 0.0064 g (0.2 mmol) elemental sulfur in 2 mL of dry oleylamine (OLA) under argon flow at 70 °C for an hour. The lead precursor was acquired separately by the dissolution of 0.28 g (1 mmol) of $PbCl_2$ in 5 mL of dry OLA at 110 °C under the argon flow for 1 h. This solution was cooled down to 70 °C and then 0.5 mL of dodecanthiol-1 was added. Finally, 2 mL of the solution of sulfur precursor (0.2 mmol of S) was injected into the $PbCl_2$ – dodecanthiol – OLA solution. The isolation of PbS CQDs was performed by the dispersion in n-hexane and precipitation with ethanol. The mean diameter of 2.5 nm and spherical shape of nanoparticles were determined by the TEM measurements. These suspensions allowed the preparation of the 100-nm thick films on the 0.15-mm thick glasses.

2.1.4 HgSe QDs

The preparation of HgSe colloidal QDs was performed using the hot-injection method. Our approach was based on the reaction of the selenium precursor with the mercury precursor prepared from mercury acetate, oleic acid, and oleylamine. The selenium precursor (TOP-Se) was prepared by adding selenium powder (0.39 g, 5 mmol) to 5 ml of trioctylphosphine (TOP) in a Schlenk tube. The mixture was stirred and heated to 70 °C for approximately 1 h to fully dissolve the selenium powder, before cooling to room temperature. The preparation of a mercury precursor based on the sequential mixing of the mercury acetate with the oleic acid and then with the oleylamine was applied.

TEM was used to determine the mean sizes and particle size distribution of the synthesized HgSe QDs. The samples prepared at 80 °C showed the 5 nm mean size of QDs with poorly formed spherical shape. The well-formed spherical QDs with a mean diameter of 7.5 nm were obtained by synthesis at 100 °C. The best particle size distribution was observed in this case. Further increase of temperature up to 120 °C led to the formation of larger nanocrystals with a mean size of 11 nm and worse particle size distribution. We used the 7.5 nm particle suspension for the dip-coating on the 0.15 mm glass plates. The thickness of the deposited films was 120 nm.

The optical densities and TEM images of QDs and NPs films are shown in Fig. 1.

2.2 Third harmonic generation set-up

We used the laser emission from the collinear optical parametric amplifier of the white light continuum (ORPHEUS-HP; 190–2500 nm spectral range, 500 kHz repetition rate, pulse energy up to 2 μJ) pumped with diode-pumped Yb femtosecond laser PHAROS PH2 (both produced by Light Conversion).

In our studies, we used the spectral range between 900 and 1700 nm with the step equal to 100 nm. The incident wavelength for the THG in the studied samples was selected in this spectral range to analyze the harmonic generation at equal energies of the driving pulses. Pulse energy was kept at 100 nJ for a whole range of spectral variations to not damage the studied samples. This energy of laser pulses

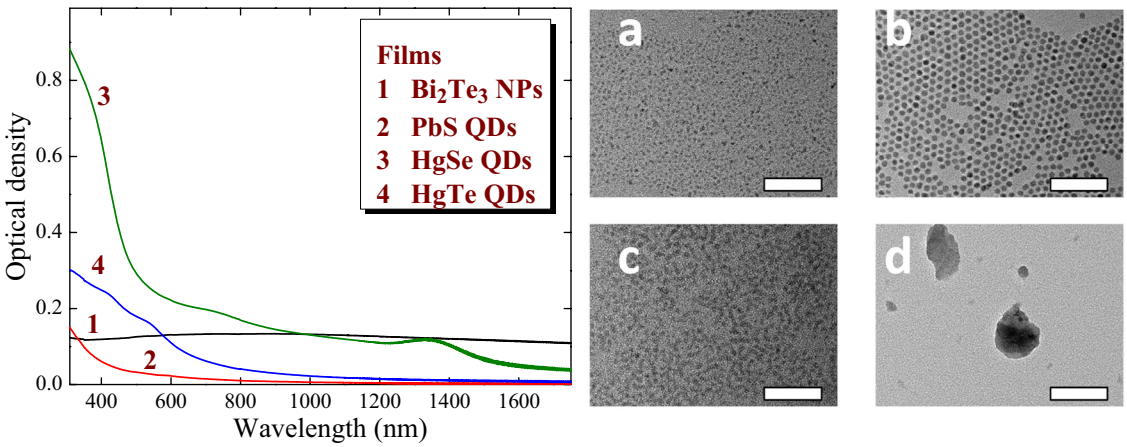

Fig. 1 Left panel: optical densities of thin films. Right panel: transmission electron microscopy images of **a** PbS QDs (mean size 2.5 nm), **b** HgSe QDs (7.5 nm), **c** HgTe QDs (4 nm), and **d** Bi_2Te_3 NPs (30–90 nm). The marked white lines correspond to 50 nm

corresponded to the intensity $I = 1.2 \times 10^{11}$ W cm^{-2}. The three-fold increase in pulse energy led to optical damage to the films. The pulse duration varied between 150 and 190 fs in the used spectral region. The width of the fundamental radiation in the focal plane was measured to be 25 μm. TH was selected using the calibrated UV and visible filters and measured by a spectrometer (Fig. 2a). The energy of laser pulses was varied using the neutral filters.

3 THG in films

In the first set of studies, we used the fixed wavelength of the fundamental radiation (1100 nm) to measure different characteristics of the THG process. We used the beam profiler (UV-NIR Beam Profiler–CinCam, CINOGY Technologies) to characterize the beam profiles. A set of ND filters was used to prevent the damage of the sensor. The spatial shapes of the fundamental and TH beams were measured at a distance of a few centimeters from the focal plane (Figs. 2b, c). The spectral shapes of TH and fundamental (1100 nm) radiation are presented in Fig. 3. Figure 3a shows the spectral shapes of TH emission measured in the case of using different films (HgTe, HgSe, Bi_2Te_3, and PbS; solid curves). We also observed THG in the silica glass plates (black dashed curve in Fig. 3a). The intensity of TH from the pure glass plate was three to six times smaller than in the case of the plates containing thin films of QDs and NPs. Notice that the ratio of the thicknesses of silica glass plate and films was 0.15 mm/100 nm = 1500.

For the lowest-order harmonic, the coherence length is defined to be in the range of a few micrometers or even larger. For example, the quasi-phase-matching in poled crystals is achieved for the flipped phases occurring at the distance of 20–30 μm in the case of second-harmonic generation. Thus for the extremely thin solid media like those used in present studies (40–120 nm) the THG can be considered as a phase-matched one along the whole length of laser beam propagation. Correspondingly, the harmonic yield should increase quadratically with the growth of the thickness of the nonlinear medium. This quadratic growth occurs until the thickness corresponding to the coherence length of TH.

To determine the exact value of the ratio of the harmonic yields from the glass and QD film of similar thicknesses one should take into account the growth of harmonic yield at the phase-matched and phase-mismatched conditions, which is a nontrivial task. However, the thickness of the glass (150 μm) was only a few times larger than the one corresponding to the lowest-order odd harmonic's coherence length. Once assuming the coherence length of TH in a glass of the order of 15 μm (i.e. 10 times thinner), the ratio of thicknesses (15 μm: 100 nm = 150) points out the at least ~ 4×10^4 ratio between the harmonic yields from these two media assuming the quadratic scaling within the coherence length.

Among the four studied materials, HgTe and HgSe showed the largest yields of TH emission at similar experimental conditions. The wavelength of TH in all these experiments with thin films was 366.5 nm, which almost corresponded to the exact position of the tripled frequency

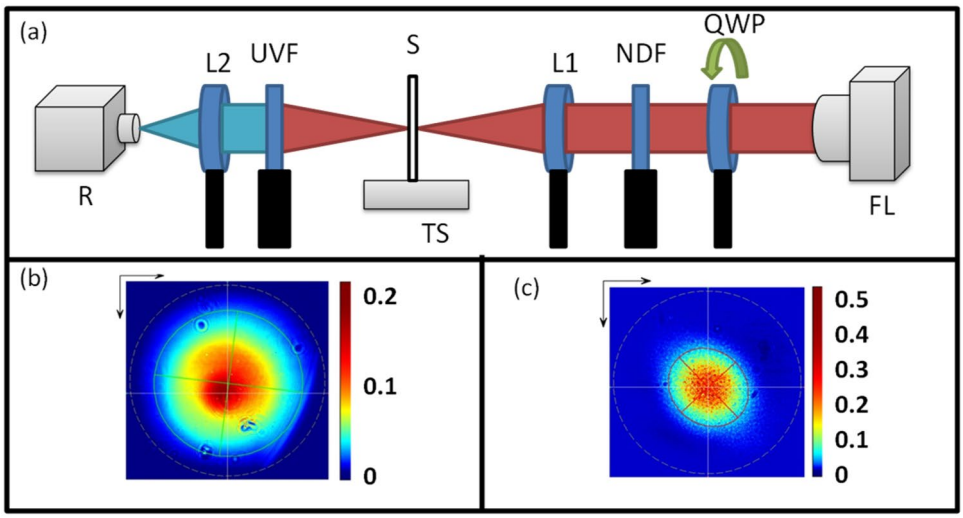

Fig. 2 **a** Experimental setup for third-harmonic generation in thin films. The description and direction of beam propagation are given from right to left. *FL* femtosecond laser (150 fs, 100 nJ, λ = 900–1700 nm, 500 kHz); *QWP* quarter-wave plate; *NDF* neutral density filters; *L*1 focusing lens; *S* sample (thin film deposited on the 0.15 mm thick silica glass plate); *TS* translating stage; *UVF* ultraviolet filter; *L*2 collecting lens; *R* registrar of TH emission (spectrometer USB 2000). **b** Spatial shape of the fundamental radiation ($\lambda = 1200$ nm). **c** Spatial shape of the TH ($\lambda = 400$ nm) in the case of HgTe film

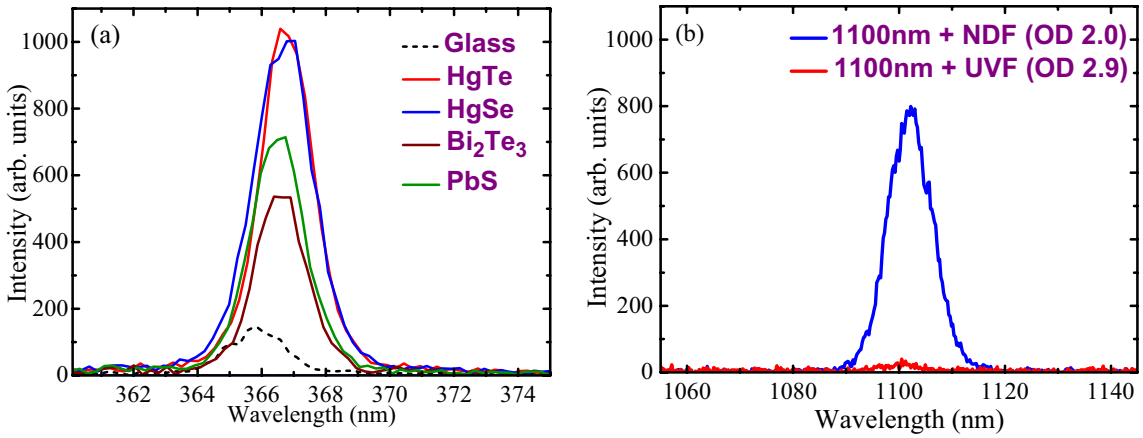

Fig. 3 Spectra of generated harmonic and fundamental radiation. **a** Third-harmonic spectra in the case of HgTe ($d=70$ nm, red curve), HgSe ($d=120$ nm, blue curve), Bi_2Te_3 ($d=50$ nm, brown curve), and PbS ($d=100$ nm, green curve) QD and NP films deposited on the 0.15 mm thick silica glass slide. **b** Spectrum of laser radiation measured using the neutral density filter (NDF, optical density 2.0 at 1100 nm, blue curve) and the ultraviolet filter (UVF, optical density 2.9 at 1100 nm, red curve)

of the laser (366.6 nm). Meanwhile, the TH from the pure glass was slightly blue-shifted (365.5 nm).

The spectral shape of the fundamental emission is shown in Fig. 3b. Here we present the spectral shapes of fundamental radiation after propagation of the neutral (blue curve) and UV (red curve) filters. The intensity of fundamental radiation in the focal plane was $I=1\times10^{11}$ W cm^{-2}. One can assume that, at this intensity, some small blue shift could be achieved during the propagation of the fundamental radiation through the relatively thick (0.15 mm) glass due to the self-modulation of propagated radiation. Meanwhile, in the case of film + glass composition, the stronger emission of TH from the ultrathin QD films was combined with the TH emission from the substrate and masked the blue shift imposed during propagation through the significantly thicker silica glass plates.

The THG signal was analyzed in the case of a few targets as a function of incident irradiance. This study showed that the slope of TH curve was close to 3, which corresponds to a third-order optical process. The conversion efficiency was calculated as follows. Due to the relatively low intensity of the TH separated after propagation of the films using UV filter the direct measurements by power meter did not allow separate it from the fundamental emission, which partially propagated through the filter. To avoid this obstacle, we measured the optical density of the UV filter at wavelengths of TH and fundamental radiation. Then the TH and fundamental emissions were collected using this filter by a calibrated spectrometer, which allowed comparing their intensities using the known transmittances of two beams through the UV filter. Correspondingly, this procedure allowed us to calculate the TH conversion efficiencies in the cases of different films.

THG conversion efficiency in the films at the used wavelength of laser radiation (1100 nm) was measured to be ~ 10^{-4}. The relatively strong conversion efficiency in such thin films can be attributed to the influence of the quantum confinement effect in the case of small-sized species like QDs when the local field can lead to the stronger nonlinear optical response of these tiny species. Smaller particles demonstrated larger values of nonlinear absorption coefficients compared with larger species of the same material. Particularly, the TH generated in the film contained large NPs (Bi_2Te_3) was weaker compared with those containing QDs, though the former film was thicker than the QDs-contained films.

The "Z-scans" of films showed a fast decrease of TH yield out of the focal plane of the focused lens (Fig. 4a). The width of those z-dependent curves was determined by the small Rayleigh length of the used fundamental radiation (0.3 mm). As already mentioned, all species followed the cubic dependence of the TH yield on the pulse energy along the whole range of the pulse energy variations (Fig. 4b).

The polarization dependencies of TH conversion efficiency showed the decay with the deviation of the polarization state from the linear to elliptical and to circular when the harmonic emission was entirely disappeared (inset to Fig. 4b). The variation of polarization was performed using the quarter-wave plate (Fig. 2a). The inset to Fig. 4b shows the dependencies of the TH yields generated in glass, HgSe, and HgTe films on the angle of a quarter-wave plate with regard to the linear polarization of laser beam. Underused experimental conditions, the measured TH intensities had an uncertainty of about 10% with the variation of the position of the quarter-wave plate. The TH yield in all cases was maximal at linear polarization (at 0°) of the laser beam, whereas it almost completely disappeared in the case of

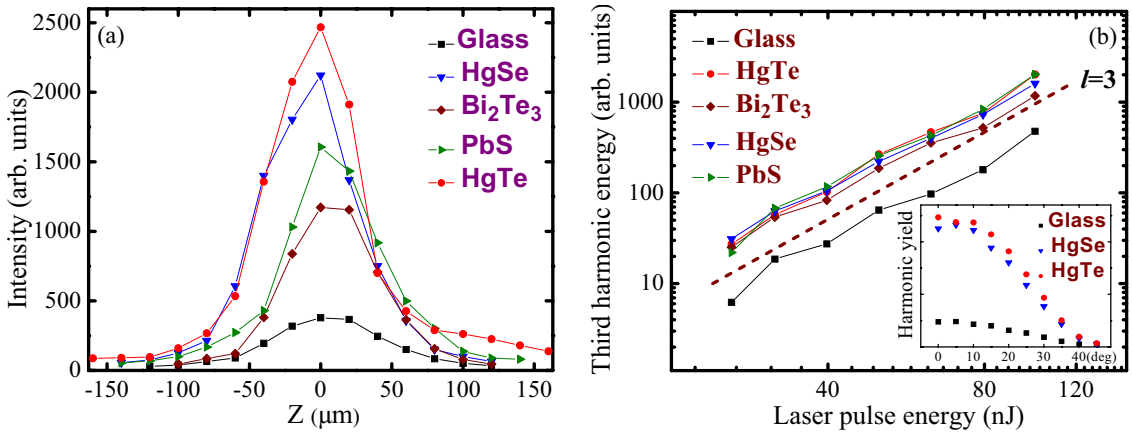

Fig. 4 Intensity dependencies of converted radiation. **a** Variations of TH intensity at different positions of films and glass with regard to the focal plane of the focusing lens ($z=0$ μm). **b** Dependences of TH energy on the energy of the driving radiation. Dotted line corresponds to the cubic slope ($l=3$). Inset: dependence of TH yield on the angle of quarter-wave plate with regard to the linear polarization

circularly polarized light (i.e. at 45° rotation of the quarter-wave plate). The variation of the TH intensity with the variation of polarization of the laser pulse is the characteristic of harmonic emission from isotropic materials, which depends as $I_{TH} \infty \cos(2\theta)$, where θ is the angle of rotation of the quarter-wave plate.

The spectral measurements of THG in thin films were carried out by tuning the wavelength of the femtosecond laser. Our laser allowed the generation of radiation in two regions (320–600 nm and 700–2200 nm, Fig. 5a). We restricted our measurements of TH to the 900 – 1700 nm spectral range of fundamental pulses variations. The reason for restricting the shorter wavelength fundamental pulses was related to the growing absorbance of the generating TH in the region below 300 nm. The limitation in the use of longer-wavelength fundamental pulses ($\lambda > 1700$ nm) was caused by the decreased yield of those pulses compared with the shorter-wavelength radiation. The used spectral range of the laser is shown as a marked rectangular area in Fig. 5a.

Figure 5a shows the images of TH (300 nm) and laser (900 nm) beams measured at the same position after the defocusing of the converting and converted radiation 100 mm from the focal plane of the focused lens. The divergence of TH was approximately three times smaller compared with the fundamental beam ($\lambda = 900$ nm). The shape of the TH beam was close to Gaussian.

The spectral-dependent measurements of the absolute values of TH conversion efficiencies along the range of tuning of the fundamental radiation were performed using the calibrated filters and spectrometer. Figure 5b shows these spectral dependencies for two films (HgTe and HgSe QDs) that demonstrated the strongest harmonic yields. The films

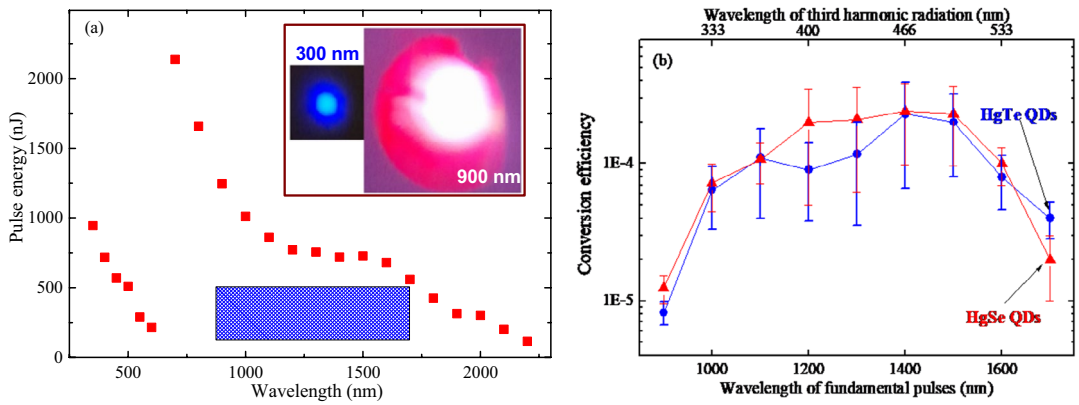

Fig. 5 **a** Output energies of pulses at different wavelengths of laser radiation. Marked rectangular area shows the spectral range of THG studies at similar energies of the fundamental pulses (100 nJ). Inset: images of 900 nm and 300 nm beams collected after the HgTe QDs sample. **b** Spectral dependencies of THG conversion efficiency in HgTe QDs film (blue-filled circles) and HgSe QDs film (red-filled triangles)

allowed achieving the 10^{-5} conversion efficiency at the shortest used wavelength ($\lambda = 900$ nm) of the fundamental radiation with further steady growth up to $\sim 2 \times 10^{-4}$ (at $\lambda = 1200$ nm). Further increase of the wavelength of fundamental radiation up to 1500 nm did not change the TH yield. At longer wavelengths of driving pulses, a decrease in harmonic yield was observed. The error factor of these measurements of the absolute value of conversion efficiency was estimated to be equal to 2.

PbS QD film was the most fragile sample among the used species. The multiple shots in the same place at longer wavelengths led to the damage, which did not allow the analysis of the dependencies of THG efficiency along the whole spectral range, though the initial shots demonstrated, as we wrote, the approximately same TH yield as for the HgTe and HgSe QD films. Bi_2Te_3 NP film was also not studied along the whole spectral range due to similar obstacles. Nevertheless, the harmonic yield in that case in some spectral ranges was only two times smaller compared with the cases of HgTe and HgSe QD films.

Considerable spectral broadening together with a blueshift of TH emission was reported in [39, 40]. However, in our case, a shift of the central wavelength of TH emission without considerable variation of spectral shape was observed only in the case of the pure silica glass substrate. The spectral width of TH emission remained constant (2.6 nm) compared with the spectral width of the driving pulses (10 nm), in a reasonable agreement with the lowest-order perturbation theory predictions ($\Delta\lambda_3 \approx 3^{-3/2}\Delta\lambda_1$).

The nonlinear dynamic scattering of the fundamental pulses could be one of the impeding factors preventing efficient THG. Meanwhile, we did not observe the nonlinear dynamic scattering during these studies. The measurements of the off-axis scattering using an additional photodiode did not allow for observing this process in the vicinity of the focal plane of the focusing lens.

A decrease of TH conversion efficiency in the case of shorter wavelength sources observed in the present study can be attributed to the growing influence of the morphological properties of the used small-sized species like size distribution and small mean size allowing expecting the involvement of strong confinement effects on the nonlinear optical properties of these species. Some additional impeding effects like growing linear absorption in the region of $\lambda < 350$ nm can also affect the TH yield. The importance of the size of the nanostructures involved in these nonlinear optical processes has been reported in a few previous studies. Particularly, in [41], a giant THG in epitaxial thin films of V–VI chalcogenide topological insulators was reported.

One can admit that, from the practical point of view, THG conversion efficiency in the so-called nonlinear crystals grown for this process is notably larger than in the low-dense isotropic media like air, laser-induced plasma, QDs- and NPs-contained thin films, etc., which do not allow the fulfillment of the phase matching between the interacting waves. The distinction between the two approaches in THG causes a large difference in the conversion efficiencies in these two cases (3×10^{-1} and 10^{-4}, respectively).

Our research was not aimed at achieving very high TH conversion efficiency in a new group of synthesized multiparticle species, but rather at a search for the evidence that those QDs and NPs possess suitable properties for the application as the media allowing the generation of the high-order harmonics. Such conditions were earlier demonstrated in the case of other QDs [42, 43]. In this connection, the practical aspects of the present work include the determination of the experimental conditions, which can be suitable for achieving the highest yield of THG.

4 Conclusions

In conclusion, we have demonstrated high conversion efficiency towards the third harmonic of the 900–1700 nm, 150 fs laser in the thin (40–120 nm) films containing the quantum dots (HgTe, HgSe, and PbS) and exfoliated nanoparticles (Bi_2Te_3) deposited on the glass substrates. The ratio of third harmonic conversion efficiencies in the films and glasses of the same thickness was calculated to be $> 10^4$. The intensity, polarization, and spectral dependencies of this process in thin films have been analyzed. The third harmonic conversion efficiency was measured to be $\sim 2 \times 10^{-4}$ in the case of HgTe and HgSe QD films. Our studies have shown that the synthesized QDs and NPs demonstrate the ability for the efficient generation of the lowest-order harmonics, which opens the doors for their application for high-order harmonics generation of ultrashort laser pulses.

Author contributions R.A.G. formulated the goal of studies. I.A.S., V.S.P., N.A.L., V.P.P., A.A.M., D.V.D, T.M. synthesized the quantum dots and nanoparticles. A.B., J.G., and A.S. carried out the characterization of the samples and laser facility. V.V.K., I.A.S., V.S.P, and A.B. carried out the nonlinear optical experiments. J.G. prepared figure 1. A.B. prepared figure 2. V.V.K prepared figures 3-5. R.A.G. wrote the main manuscript text. All authors reviewed the manuscript.

Funding European Regional Development Fund (1.1.1.5/19/A/003), Horizon 2020 Framework Programme (739508).

Declarations

Conflict of interest The authors declare no competing interests.

References

1. M. Chen, G. Shen, P. Guyot-Sionnest, J. Phys. Chem. C **124**, 16216 (2020)

2. P. Klenovský, A. Schliwa, D. Bimberg, Phys. Rev. B **100**, 115424 (2019)
3. P. Klenovský, J. Valdhans, L. Krejčí, M. Valtr, P. Klapetek, O. Fedotova, Electron. Struct. **4**, 015006 (2022)
4. P. Klenovský, M. Brehm, V. Křápek, E. Lausecker, D. Munzar, F. Hackl, H. Steiner, T. Fromherz, G. Bauer, J. Humlíček, Phys. Rev. B **86**, 115305 (2012)
5. P. Klenovský, D. Hemzal, P. Steindl, M. Zíková, V. Křápek, J. Humlíček, Phys. Rev. B **92**, 241302 (2015)
6. H. Huang, D. Csontosová, S. Manna, Y. Huo, R. Trotta, A. Rastelli, P. Klenovský, Phys. Rev. B **104**, 165401 (2021)
7. D. Csontosová, P. Klenovský, Phys. Rev. B **102**, 125412 (2020)
8. P. Klenovský, P. Baranowski, P. Wojnar, Phys. Rev. B **105**, 195403 (2022)
9. F.W. Wise, Acc. Chem. Res. **33**, 773 (2000)
10. I. Karabulut, H. Şafak, M. Tomak, J. Phys. D **41**, 155104 (2008)
11. T.S. Kondratenko, A.I. Zvyagin, M.S. Smirnov, I.G. Grevtseva, A.S. Perepelitsa, O.V. Ovchinnikov, J. Lumin. **208**, 193 (2019)
12. J. Szeremeta, M. Nyk, D. Wawrzynczyk, M. Samoc, Nanoscale **5**, 2388 (2013)
13. D.D. Kohler, B.J. Thompson, J.C. Wright, J. Phys. Chem. C **122**, 18086 (2018)
14. M. Molaei, M. Karimipour, S. Abbasi, M. Khanzadeh, M. Dehghanipour, J. Mater. Res. **35**, 401 (2020)
15. M.S. Neo, N. Venkatram, G.S. Li, W.S. Chin, W. Ji, J. Phys. Chem. C **114**, 18037 (2010)
16. I.D. Skurlov, E.A. Ponomareva, A.O. Ismagilov, S.E. Putilin, I.A. Vovk, A.V. Sokolova, A.N. Tcypkin, A.P. Litvin, Photonics **7**(2), 39 (2020)
17. X. Li, C. Chang, Opt. Mater. **131**, 112605 (2022)
18. H. Dakhlaoui, A.S. Durmuslar, I. Rodriguez-vargas, F. Ungan, Eur. Phys. J. Plus **137**, 526 (2022)
19. H. Yu, Z. Zhen, Y.-S. Shi, K.-X. Guo, E. Feddi, J.-H. Yuan, Z.-H. Zhang, Eur. Phys. J. Plus **137**, 555 (2022)
20. R. Karimzadeh, H. Aleali, N. Mansour, Opt. Commun. **284**, 2370 (2011)
21. Z. Zeng, C.S. Garoufalis, A.F. Terzis, S. Baskoutas, J. Appl. Phys. **114**, 023510 (2013)
22. L. Miao, J. Yi, Q. Wang, D. Feng, H. He, S. Lu, C. Zhao, H. Zhang, S. Wen, Opt. Mater. Express **6**, 2244 (2016)
23. J. Qiao, M.-Y. Chuang, J.-C. Lan, Y.-Y. Lin, W.-H. Sung, R. Fan, M.-Y. Wu, C.-Y. Lee, C.-H. Chen, H. Liu, C.-K. Lee, J. Mater. Chem. C **7**, 7027 (2019)
24. J.-C. Lan, J. Qiao, W.-H. Sung, C.-H. Chen, R.-H. Jhang, S.-H. Lin, L.-R. Ng, G. Liang, M.-Y. Wu, L.-W. Tu, C.-M. Cheng, H. Liu, C.-K. Lee, Nanoscale **12**, 16956 (2020)
25. D. Liu, C. He, L. Chen, W. Li, Y. Zu, Opt. Mater. **111**, 110634 (2021)
26. S. Backus, J. Peatross, Z. Zeek, A. Rundquist, G. Taft, M.M. Murnane, H.C. Kapteyn, Opt. Lett. **21**, 665 (1996)
27. R.A. Ganeev, M. Suzuki, M. Baba, H. Kuroda, I.A. Kulagin, Appl. Opt. **45**, 748 (2006)
28. S. Suntsov, D. Abdollahpour, D.G. Papazoglou, S. Tzortzakis, Opt. Express **17**, 3190 (2009)
29. R.A. Ganeev, H. Singhal, P.A. Naik, J.A. Chakera, M. Kumar, P.D. Gupta, Phys. Rev. A **82**, 043812 (2010)
30. M. Stafe, C. Negutu, N.N. Puscas, Appl. Phys. B **124**, 106 (2018)
31. H. Yang, J. Zhang, J. Zhang, L.Z. Zhao, Y.J. Li, H. Teng, Y.T. Li, Z.H. Wang, Z.L. Chen, Z.Y. Wei, J.X. Ma, W. Yu, Z.M. Sheng, Phys. Rev. E **67**, 015401 (2003)
32. F. Théberge, N. Aközbek, W. Liu, J.-F. Gravel, S.L. Chin, Opt. Commun. **245**, 399 (2005)
33. G.S. Boltaev, N.A. Abbasi, V.V. Kim, M. Iqbal, S.A. Khan, A.I. Zvyagin, M.S. Smirnov, O.V. Ovchinnikov, R.A. Ganeev, A.S. Alnaser, Appl. Phys. B **126**, 76 (2020)
34. A.B. Fedotov, N.I. Koroteev, M.M.T. Loy, X. Xiao, A.M. Zheltikov, Opt. Commun. **133**, 587 (1997)
35. N. Aközbek, A. Iwasaki, A. Becker, M. Scalora, S.L. Chin, C.M. Bowden, Phys. Rev. Lett. **89**, 143901 (2002)
36. M.L. Naudeau, R.J. Law, T.S. Luk, T.R. Nelson, S.M. Cameron, J.V. Rudd, Opt. Express **14**, 6194 (2006)
37. R.A. Ganeev, V.S. Popov, A.I. Zvyagin, N.A. Lavrentyev, A.E. Mirofyanchenko, E.V. Mirofyanchenko, I.A. Shuklov, O.V. Ovchinnikov, V.P. Ponomarenko, V.F. Razumov, Nanophot. **10**, 3857 (2021)
38. A. Bundulis, I.A. Shuklov, V.V. Kim, A. Mardini, J. Grube, J. Alnis, A.A. Lizunova, V.F. Razumov, R.A. Ganeev, Nanomater. **11**, 3351 (2021)
39. J. Peatross, S. Baskus, J. Zhou, M.M. Murnane, H.C. Kapteyn, J. Opt. Soc. Am. B **15**, 186 (1998)
40. G. Marcus, A. Zigler, Z. Henis, J. Opt. Soc. Am. B **16**, 792 (1999)
41. Y. Xiang, C. Yan, T.D. Stanescu, Y. Ma, R. Sooriyagoda, F. Shi, A.D. Bristow, L. Li, C. Cen, Nano Lett. **21**, 8872 (2012)
42. R.A. Ganeev, G.S. Boltaev, V.V. Kim, K. Zhang, A.I. Zvyagin, M.S. Smirnov, O.V. Ovchinnikov, P.V. Redkin, M. Wöstmann, H. Zacharias, C. Guo, Opt. Express **26**, 35013 (2018)
43. R.A. Ganeev, G.S. Boltaev, V.V. Kim, M. Venkatesh, A.I. Zvyagin, M.S. Smirnov, O.V. Ovchinnikov, M. Wöstmann, H. Zacharias, C. Guo, J. Appl. Phys. **126**, 193103 (2019)